NMR study of nematic spin fluctuations in a detwinned single crystal of underdoped $Ba(Fe_{1-x}Co_x)_2As_2$

T. Kissikov,[1] A. P. Dioguardi,[2] E. I. Timmons,[3] M. A. Tanatar,[3] R. Prozorov,[3] S. L. Bud'ko,[3] P. C. Canfield,[3] R. M. Fernandes,[4] and N. J. Curro[1]

[1]*Department of Physics, University of California, Davis, California 95616, USA*

[2]*Condensed Matter and Magnet Science, Los Alamos National Laboratory, Los Alamos, New Mexico 87545, USA*

[3]*Ames Laboratory, U.S. Department of Energy, and Department of Physics and Astronomy, Iowa State University, Ames, Iowa 50011, USA*

[4]*School of Physics and Astronomy, University of Minnesota, Minneapolis, Minnesota 55116, USA*

(Received 12 August 2016; revised manuscript received 21 September 2016; published 11 October 2016)

We report the experimental details of how mechanical detwinning can be implemented in tandem with high-sensitivity nuclear magnetic resonance measurements and use this setup to measure the in-plane anisotropy of the spin-lattice relaxation rate in underdoped $Ba(Fe_{1-x}Co_x)_2As_2$ with $x = 0.048$. The anisotropy reaches a maximum of 30% at T_N, and the recovery data reveal that the glassy behavior of the spin fluctuations present in the twinned state persist in the fully detwinned crystal. A theoretical model is presented to describe the spin-lattice relaxation rate in terms of anisotropic nematic spin fluctuations.

DOI: 10.1103/PhysRevB.94.165123

I. INTRODUCTION

The iron pnictide superconductors exhibit rich phase diagrams with several competing electronic phases [1,2]. The parent undoped materials are tetragonal paramagnets at high temperature, but undergo an orthorhombic structural distortion prior to, or coincident with, long-range antiferromagnetic order of the Fe moments at low temperature. With electron or hole doping, the structural and magnetic ordering temperatures are suppressed, and for sufficiently high doping levels superconductivity emerges, often manifesting a maximum in transition temperature, T_c, near the boundary of the orthorhombic-antiferromagnetic phase. Although this phase diagram is similar to other unconventional superconductors, questions that have remained open in the pnictides are whether the antiferromagnetic fluctuations play a role in the superconducting mechanism and how these competing phases are related to the orthorhombic distortion [3–6].

The tetragonal-to-orthorhombic transition at T_s is driven by an electronic nematic instability that breaks the C_4 point group symmetry of the lattice [7–9]. The microscopic origin of this nematic instability has been the subject of intense debate—in particular, whether it arises from spin or orbital degrees of freedom (for a review, see Ref. [10]). In the nematic phase, stripelike magnetic order sets in at a temperature $T_N \leqslant T_s$, with the moments ordered ferromagnetically along the b_O direction and antiferromagnetically along $a_O > b_O$ (see Fig. 1) [11,12]. In the absence of strain, orthorhombic distortions can occur along any of the two degenerate directions, leading to twin domains in bulk crystals [13,14]. Twinning therefore precludes measurements of anisotropic behavior in the ab plane, since the crystal contains nominally equal populations of all such domains. On the other hand, cooling through the structural transition while maintaining uniaxial stress along the $(100)_O$ direction can nucleate single domains [15,16]. Strain, therefore, provides an avenue to uncover the intrinsic planar anisotropy in detwinned crystals. Transport and neutron scattering studies under elastic strain have uncovered large nematic correlations both in the charge and spin degrees of freedom [7,17–19]. These nematic fluctuations diverge at T_s and persist well into the paramagnetic tetragonal phase. Angle-resolved photoemission [20] and infrared optical reflection spectroscopy [21] studies have also been conducted on detwinned crystals, revealing a distinct Fermi surface anisotropy both above and below the structural transition of the unstrained sample.

Nuclear magnetic resonance (NMR) of the ^{75}As offers detailed information about the temperature dependence of these spin fluctuations and their doping dependence [22–28]. A recent NMR study in underdoped $Ba(Fe_{1-x}Co_x)_2As_2$ revealed that critical slowing down sets in at T_s; however, these crystals remained twinned and therefore no information about the anisotropy of these critical fluctuations was available [29]. NMR studies have also uncovered significant dynamical inhomogeneity in $Ba(Fe_{1-x}Co_x)_2As_2$, giving rise to stretched exponential relaxation observed in the spin-lattice relaxation rate [30–33]. The crystals in these studies also remained twinned, and an open question is whether the intrinsic spin fluctuations are sufficiently anisotropic to explain the broad range of spin-lattice relaxation rates observed in the presence of multiple twin domains.

Here we report NMR measurements on a detwinned single crystal of $Ba(Fe_{1-x}Co_x)_2As_2$ with $x = 0.048$ suspended across a mechanical horseshoe clamp. NMR results under uniaxial stress in these materials have not been reported previously. Spin-lattice relaxation rate measurements in twinned samples include contributions from both domains simultaneously, and therefore the magnetization recovery may consist of a distribution of relaxation rates [32]. The material studied here is underdoped, with $T_s \approx 60$ K, $T_N \approx 50$ K, and $T_c \approx 18$ K. We find that the spin lattice relaxation rate is anisotropic in the basal plane, reflecting strong nematic spin correlations of the Fe spins extending above T_s. We also find that the stretched exponential recovery persists in the detwinned crystals. These results suggest that random strain fields induced by the dopants is greater than the externally applied strain used to detwin the crystal. The paper is organized as follows: Section II describes the strain device and resistivity measurements, Sec. III describes the spin-lattice relaxation measurements, and Sec. IV describes the interpretation of the relaxation rate data in terms of nematic spin fluctuations. Details of the calculation

of T_1^{-1} in terms of the dynamical spin susceptibility are given in the appendix.

II. APPLICATION OF STRAIN AND DETWINNING

Single crystals were synthesized via a self-flux method and characterized via transport measurements and wavelength-dispersive spectroscopy to determine the Co-doping level [34]. A sample of dimensions 1.1 mm × 0.57 mm × 0.05 mm was cut with the long axis parallel to the tetragonal [110] direction, and mounted in a mechanical horseshoe device as described in Ref. [16] and shown in Fig. 1. The crystal was secured using silver wires soldered to the edges of the sample. These wires serve not only to transmit tensile stress to the crystal but also as leads for resistivity measurements. Stress is applied by tightening a screw by about 1/4 to 1/2 turn, which is enough to apply stresses on the order of 10–20 MPa [16]. The sample was inserted into the NMR coil embedded in epoxy prior to mounting in the clamp cell. This is the first time such a device has been employed for NMR measurements.

The resistance of the crystal is shown in Fig. 2 as a function of temperature measured in zero magnetic field. In the unstrained state, the resistivity exhibits a minimum at T_s, and the temperature derivative dR/dT curve exhibits a broad maximum close to T_N [1,34]. Note, however, that we identify T_N not by the resistance measurements, but by the peak in T_1^{-1}, as discussed below, since that indicates a divergence in the

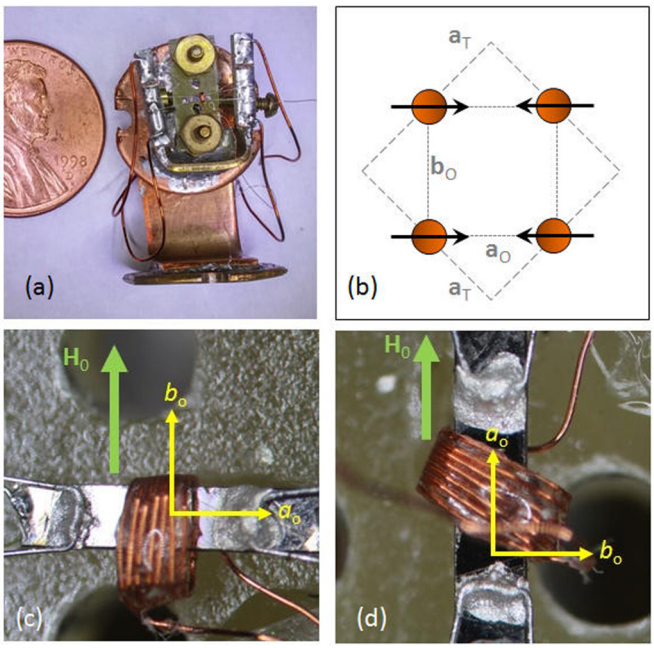

FIG. 1. (a) Strain device with single crystal of $Ba(Fe_{0.952}Co_{0.048})_2As_2$ under strain. (b) *ab* plane, showing the Fe atoms and spin orientation in the ordered magnetic phase, with the orthorhombic a_O and b_O axes shown as dotted lines, and the tetragonal axes (a_T) shown as dashed lines. (c) Close-up image of the crystal oriented such that the applied field, $\mathbf{H}_0$, is along the b_O (perpendicular to the direction of applied strain) and (d) along a_O (parallel to the direction of applied strain). For the latter case, the coil was rotated by approximately 30° so that a component of the radio-frequency field $\mathbf{H}_1$ lies perpendicular to $\mathbf{H}_0$.

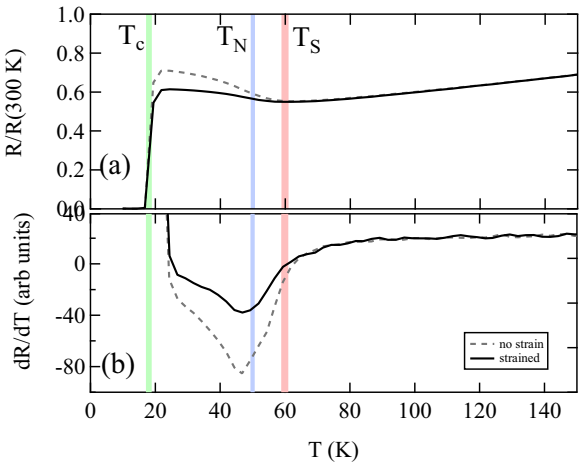

FIG. 2. (a) Resistance and (b) derivative of resistance versus temperature for the $Ba(Fe_{0.952}Co_{0.048})_2As_2$ crystal measured with and without strain in zero field. Resistivity reaches a minimum at T_S, and the dR/dT curve exhibits a minimum at T_N [1].

critical spin fluctuations. In the absence of strain, the resistance includes domains oriented both along the crystallographic a_O and b_O directions. Under strain, domains oriented with the a_O axis parallel to the direction of applied tensile strain are favored, and the measured resistance changes below T_s. For sufficiently large strain, the measured resistance becomes independent of strain, indicating a fully detwinned state. Figure 2 shows the resistance for the fully detwinned state. This behavior is consistent with independent measurements of the resistivity along the a_O direction [15].

III. SPIN-LATTICE RELAXATION

The spin-lattice relaxation rate, T_1^{-1}, was measured at the central transition of the ^{75}As ($I = 3/2$) by inversion recovery in a field of $H_0 = 11.73$ T for the field perpendicular to the c axis, with and without strain applied. The measurements were conducted with $\mathbf{H}_0$ oriented both parallel ($\mathbf{H}_0||\hat{a}_0$) and perpendicular ($\mathbf{H}_0||\hat{b}_0$) to the direction of applied strain. The nuclear magnetization was fit to a stretched exponential, $M(t) = M_0[1 - f\{9\exp[-(6t/T_1)^\beta]/10 + \exp[-(t/T_1)^\beta]\}/10]$, where M_0 is the equilibrium magnetization, f is the inversion fraction, and β is the stretching exponent [32]. $(T_1T)^{-1}$ and β are shown as a function of temperature in Fig. 3 (note that the data have been offset vertically for clarity). For $\mathbf{H}_0||\hat{b}_0$, the coil was naturally oriented such that the rf field $\mathbf{H}_1 \perp \mathbf{H}_0$, as shown in Fig. 1(c); this condition is necessary in order to detect the nuclear magnetization. For $\mathbf{H}_0||\hat{a}_0$ the coil was rotated by ~30° from the strain axis as shown in Fig. 1(d) in order to create a component of $\mathbf{H}_1$ that is perpendicular to $\mathbf{H}_0$. The clamp and suspended crystal were warmed to room temperature and rotated between Figs. 1(c) and 1(d). Because the applied stress was not changed, the level of strain was nominally identical for the two orientations. The component parallel to $\mathbf{H}_0$ has no effect on the nuclear magnetization and does not affect the T_1^{-1} measurement.

As seen in Fig. 3, the relaxation rate diverges at T_N, and the stretching exponent, β, reaches a minimum of ≈0.5 at

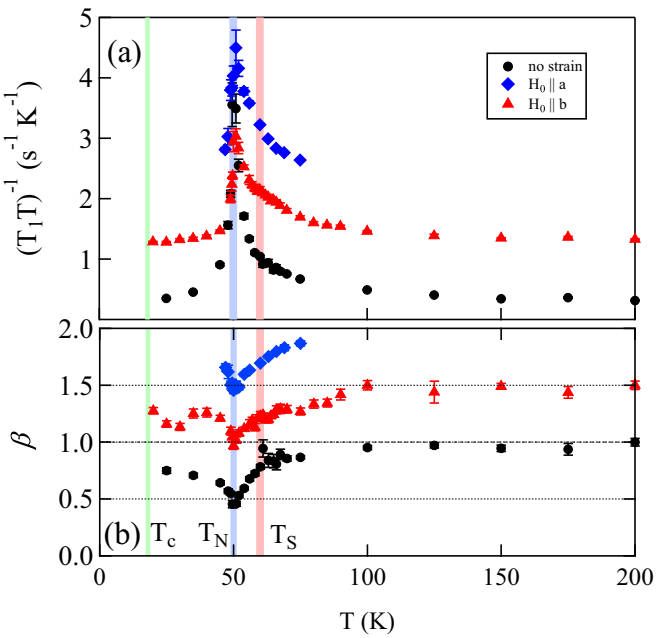

FIG. 3. (a) $(T_1T)^{-1}$ and (b) the stretching exponent β vs temperature for $Ba(Fe_{0.952}Co_{0.048})_2As_2$ for field oriented along either the a_O or b_O directions. The data in panel (a) have been offset vertically by 1 and 2 $s^{-1}K^{-1}$ for clarity and in panel (b) by 0.5 and 1.0.

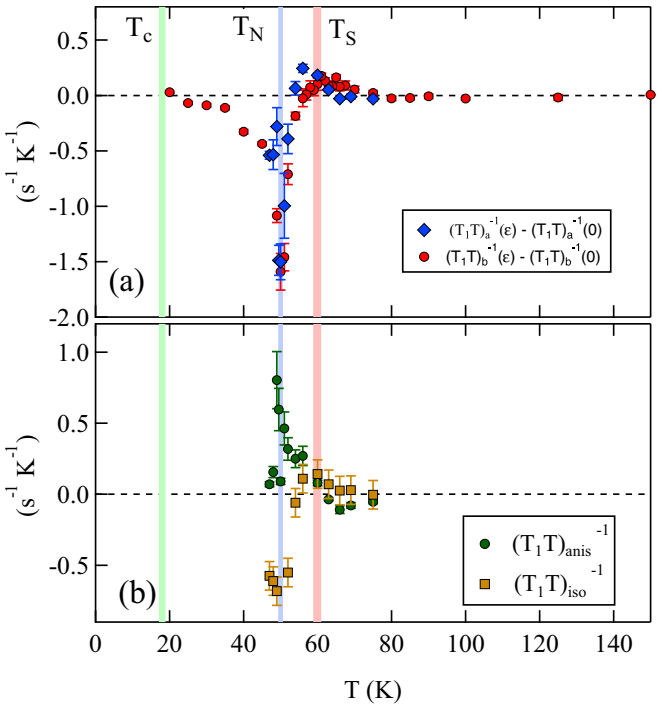

FIG. 4. (a) $(T_1T)^{-1}(\epsilon) - (T_1T)^{-1}(0)$ for field along both the a and b directions, and (b) $(T_1T)^{-1}_{\rm anis}$ and $(T_1T)^{-1}_{\rm iso}$ vs temperature for $Ba(Fe_{0.952}Co_{0.048})_2As_2$.

this temperature. The same qualitative behavior is observed with and without strain, but there are subtle differences in $(T_1T)^{-1}$ that emerge near T_s under strain. The peak value of $(T_1T)^{-1}$ decreases by ~30% for both directions under strain. Furthermore, the data for $\mathbf{H}_0||\hat{b}_0$ appears to exhibit a small shoulder at T_S that does not appear in the data for the a_O direction. Surprisingly β does not show any significant differences under strain. β is a direct measure of the width of the distribution of local relaxation rates [35]. This distribution has been postulated to arise from random strain fields induced by the dopants that couple to nematic order, causing β to decreases from unity below a temperature on the order of 100 K in this doping range [30]. This inhomogeneity might be expected to vanish in the presence of a homogeneous strain field that is enough to induce a single nematic domain. However, the data indicate that the level of inhomogeneity, as measured by the size of β, remains unchanged. This result suggests that either the origin of the inhomogeneous relaxation arises from some other source of disorder or that the random strain fields induced by the Co dopant atoms [36], which are much larger than the modest homogenous strain field that is applied to detwin the crystal, are responsible for the glassy behavior.

Figure 4(a) shows the difference $\Delta(T_1T)^{-1}_\alpha = (T_1T)^{-1}_\alpha(\varepsilon) - (T_1T)^{-1}_\alpha(0)$ $(\alpha = a,b)$ between the relaxation rates with and without uniaxial tensile strain for both directions. Figure 4(b) shows the anisotropy in the relaxation rate, $(T_1T)^{-1}_{\rm anis} = (T_1T)^{-1}_a - (T_1T)^{-1}_b$ under strain, and the isotropic strain-induced component, $(T_1T)^{-1}_{\rm iso} = \frac{1}{2}[(T_1T)^{-1}_a(\epsilon) + (T_1T)^{-1}_b(\epsilon)] - (T_1T)^{-1}(0)$. The relaxation was measured for both crystal directions in the absence of strain, and no differences were observed to within the error bars. All of these quantities peak at T_N, but remain finite up to and above T_s. This behavior reflects the fact that C_4 symmetry is broken by the strain field, which induces a finite nematicity above the onset of long-range nematic order, similarly to how a magnetic field induces a finite magnetization in the paramagnetic phase above the Curie temperature in a ferromagnet. Similar behavior has been observed in elastoresistance and neutron scattering measurements [7,17,18]. Note that the magnitude of $(T_1T)^{-1}_{\rm anis}$ in the detwinned state is approximately 30% of the value of $(T_1T)^{-1}$ in the unstrained state at T_N. The width of the distribution of relaxation rates, however, far exceeds this variation due to the anisotropy, which is consistent with the observation that β is unchanged in the detwinned state.

IV. ANALYSIS

To analyze the results, we start with the general expression for the spin-lattice relaxation rate due to a magnetic field applied in an arbitrary direction. Hereafter, our coordinate system refers to the 1-Fe unit cell in the orthorhombic phase. In the paramagnetic state, the internal field experienced by the nucleus is zero and we obtain [37]

$$\left(\frac{1}{T_1T}\right)_{\theta,\phi} = \frac{g^2}{2}\sum_{\mathbf{q}}\sum_{i=1,2}[\bar{R}\cdot\bar{A}_{\mathbf{q}}\cdot\bar{\tilde{\chi}}(\mathbf{q})\cdot\bar{A}^{\dagger}_{\mathbf{q}}\cdot\bar{R}^{\dagger}]_{ii}, \quad (1)$$

where g is a constant proportional to the gyromagnetic ratio of the nucleus, $\bar{A}_{\mathbf{q}}$ is the hyperfine tensor (shown explicitly in the appendix), $\bar{R}$ is the rotation matrix (shown explicitly in the appendix), and θ,φ are the polar and azimuthal angles describing the direction of the magnetic field with respect to the (a,b,c) crystal axis. In this coordinate system, the susceptibility is di-

agonal in spin space, $\bar{\chi} = \mathrm{diag}(\chi_{aa}, \chi_{bb}, \chi_{cc})$. For convenience, we defined $\tilde{\chi}_{\alpha\beta}(\mathbf{q}) = \lim_{\omega\to 0} \frac{\mathrm{Im}\chi_{\alpha\beta}(\mathbf{q},\omega)}{\omega}$. Because the system is metallic, Landau damping γ is present and we can write $\chi^{-1}_{\alpha\beta}(\mathbf{q},\omega) = \chi^{-1}_{\alpha\beta}(\mathbf{q}) - i\gamma\omega$, yielding $\tilde{\chi}_{\alpha\beta}(\mathbf{q}) = \gamma\chi^2_{\alpha\beta}(\mathbf{q})$.

The anisotropy in the spin-lattice relaxation rate $(\frac{1}{T_1T})_{\mathrm{anis}} \equiv (\frac{1}{T_1T})_a - (\frac{1}{T_1T})_b \equiv (\frac{1}{T_1T})_{\phi=0,\theta=\pi/2} - (\frac{1}{T_1T})_{\phi=\pi/2,\theta=\pi/2}$ can be calculated directly from Eq. (1). In general, the anisotropy in $1/T_1T$ can arise from two sources: either an anisotropy in the elements of the hyperfine tensor $\bar{A}_{\mathbf{q}}$ or an anisotropy in the elements of the susceptibility tensor $\chi_{\alpha\beta}$. The latter reflects the anisotropies of the magnetic fluctuations, whereas the former is mainly determined by the changes in the lattice environment. Since the lattice distortions are very small, hereafter we focus on the anisotropies induced by the spin spectrum only, setting $A_{aa} = A_{bb}$, $A_{bc} = A_{ac}$, and $A_{ab} = A_{ba}$. We obtain

$$\left(\frac{1}{T_1T}\right)_{\mathrm{anis}} = \frac{g^2}{2}\sum_{\mathbf{q}}\left\{\left[F_1(\mathbf{q})A^2_{ab} - F_2(\mathbf{q})A^2_{aa}\right] \times \left[\tilde{\chi}_{aa}(\mathbf{q}) - \tilde{\chi}_{bb}(\mathbf{q})\right] + F_3(\mathbf{q})A^2_{ac}\tilde{\chi}_{cc}(\mathbf{q})\right\} \quad (2)$$

with the form factors $F_1(\mathbf{q}) = \sin^2(\frac{q_x}{2})\sin^2(\frac{q_y}{2})$, $F_2(\mathbf{q}) = \cos^2(\frac{q_x}{2})\cos^2(\frac{q_y}{2})$, and $F_3(\mathbf{q}) = \frac{1}{2}(\cos q_x - \cos q_y)$. The existence of a sizable spin-orbit coupling in the iron pnictides [38] enforces important symmetry constraints on the susceptibility tensor [39,40]. Specifically, in the tetragonal paramagnetic phase, while $\chi_{aa}(\mathbf{q})$ and $\chi_{bb}(\mathbf{q})$ do not need to be C_4 (tetragonal) symmetric functions, $\chi_{aa}(\mathbf{q})$ becomes identical to $\chi_{bb}(\mathbf{q})$ upon a 90° rotation. Therefore, because the combination $\tilde{\chi}_{aa}(\mathbf{q}) - \tilde{\chi}_{bb}(\mathbf{q})$ is C_2 symmetric, while the functions $F_1(\mathbf{q})$ and $F_2(\mathbf{q})$ are C_4 symmetric, the first term in Eq. (2) vanishes in the tetragonal phase. Similarly, symmetry requires that $\chi_{cc}(\mathbf{q})$ is a C_4 symmetric function; thus, because $F_3(\mathbf{q})$ is C_2 symmetric, the second term vanishes as well. Hence, as expected, $(T_1T)^{-1}_{\mathrm{anis}}$ vanishes in the tetragonal phase.

To model the magnetic spectrum of the pnictides, we note that at low energies the susceptibility is strongly peaked at the magnetic ordering vectors $\mathbf{Q}_1 = (\pi,0)$ and $\mathbf{Q}_2 = (0,\pi)$, as seen by neutron scattering [41,42]. If the susceptibilities were δ functions peaked at the ordering vectors, then the fact that $F_1(\mathbf{Q}_i) = F_2(\mathbf{Q}_i) = 0 \neq F_3(\mathbf{Q}_i)$ would imply that $(T_1T)^{-1}_{\mathrm{anis}}$ probes only the χ_{cc} component of the susceptibility tensor. However, the system has a finite magnetic correlation length in the paramagnetic phase. To model this behavior, we consider a low-energy model in which the susceptibilities are peaked at the magnetic ordering vectors [43]:

$$\begin{aligned}
\frac{\chi_{aa}(\mathbf{q})}{\chi_0} &= \left(\xi_1^{-2} + \cos q_x - \cos q_y + 2\right)^{-1} \\
&\quad + \left(\xi_2^{-2} - \cos q_x + \cos q_y + 2\right)^{-1}, \\
\frac{\chi_{bb}(\mathbf{q})}{\chi_0} &= \left(\xi_2^{-2} + \cos q_x - \cos q_y + 2\right)^{-1} \\
&\quad + \left(\xi_1^{-2} - \cos q_x + \cos q_y + 2\right)^{-1}, \\
\frac{\chi_{cc}(\mathbf{q})}{\chi_0} &= \left(\xi_3^{-2} + \cos q_x - \cos q_y + 2\right)^{-1} \\
&\quad + \left(\xi_3^{-2} - \cos q_x + \cos q_y + 2\right)^{-1}, \qquad (3)
\end{aligned}$$

where we defined the correlation lengths ξ_i associated with each magnetic channel (in units of the lattice constant a) and the magnetic energy scale χ_0^{-1}. In the tetragonal phase, symmetry requires that $\chi_{aa}(\mathbf{Q}_1) = \chi_{bb}(\mathbf{Q}_2)$, $\chi_{bb}(\mathbf{Q}_1) = \chi_{aa}(\mathbf{Q}_2)$, and $\chi_{cc}(\mathbf{Q}_1) = \chi_{cc}(\mathbf{Q}_2)$ [40], which is satisfied by Eq. (3). The situation is different in the nematic phase, where magnetic fluctuations become anisotropic; i.e., fluctuations around $\mathbf{Q}_1$ and $\mathbf{Q}_2$ are no longer equivalent. Because the susceptibility tensor has three independent elements, one needs to introduce three so-called nematic order parameters φ_i, with $i = 1,2,3$. We introduce them in Eq. (3) by replacing the magnetic correlation lengths $\xi_1^{-2} \to \xi_1^{-2} \mp \varphi_1$, $\xi_2^{-2} \to \xi_2^{-2} \pm \varphi_2$ (where the upper sign refers to χ_{aa} whereas the lower sign refers to χ_{bb}), and $\xi_3^{-2} \to \xi_3^{-2} \mp \varphi_3$ (where the upper sign corresponds to the first term in χ_{cc} whereas the lower sign refers to the second term). The physical meaning of these nematic order parameters is clear [8], as $\varphi_i > 0$ ($\varphi_i < 0$) implies that the $\mathbf{Q}_1(\mathbf{Q}_2)$ ordering vector is selected in the nematic phase. The fact that these three order parameters break the same symmetry implies that they are either all zero or all nonzero (i.e., $\varphi_1 \propto \varphi_2 \propto \varphi_3$); however, their relative signs depend on microscopic considerations.

Substituting these expressions in Eq. (2) and expanding to leading order in the three nematic order parameters, we obtain (in units of $\frac{g^2\gamma\chi_0}{\pi}$)

$$(T_1T)^{-1}_{\mathrm{anis}} = -2\left(A^2_{aa} - A^2_{ab}\right)\left(\varphi_1\xi_1^2 - \varphi_2\xi_2^2\right) - 8A^2_{ac}\varphi_3\xi_3^4 \quad (4)$$

and

$$\Delta(T_1T)^{-1}_{\mathrm{iso}} = 8A^2_{ac}\xi_1^6\varphi_1^2 + \tfrac{1}{2}\left(A^2_{aa} + A^2_{ab}\right)\xi_2^4\varphi_2^2 + 4A^2_{ac}\xi_3^6\varphi_3^2. \quad (5)$$

In deriving these expressions, we considered ξ_i to be moderately large and kept the leading order terms for each ξ_i. We also neglected any strain-induced changes to the tetragonal hyperfine coupling tensor. As expected by symmetry consideration, $(T_1T)^{-1}_{\mathrm{anis}}$ varies linearly with φ_i, whereas $\Delta(T_1T)^{-1}_{\mathrm{iso}}$ varies quadratically. According to previous NMR investigations, $A_{aa} \approx 0.66$ kOe/μ_B and $A_{ac} \approx 0.43$ kOe/μ_B [23]. We do not have direct information about A_{ab}; however, all of the other elements of the hyperfine tensor are known. If we assume that one of the principal axes of the tensor lies along the Fe-As bond axis, then we can constrain $A_{ab}/A_{aa} = 0.37$ or -0.94; thus it is reasonable to assume $A_{ab} < A_{aa}$.

We are now in a position to analyze the experimental results displayed in Fig. 4. The presence of tensile strain ε along the a axis effectively induces a conjugate field that couples to the nematic order parameters, i.e., $\varphi_i \propto \varepsilon$. As a result, the nematic phase extends to high temperatures, and T_S signals a crossover rather than an actual phase transition. Furthermore, because in our experiment tensile strain is applied along the a axis, the $\mathbf{Q}_1$ ordering vector is selected by the external strain, with spins pointing along the a axis (see Fig. 1 and also Ref. [17]). As a result, $\varphi_1 > 0$, although φ_2 and φ_3 could in principle have different signs.

At temperatures much larger than the magnetic transition temperature T_N, the effects of the spin-orbit coupling are presumably small. Therefore, in this regime, the magnetic

spectrum should display an isotropic behavior, with $\xi_i \approx \xi$. In this regime the last term in Eq. (4) dominates, and the sign of $(T_1T)^{-1}_{\rm anis}$ is the opposite as the sign of φ_3. According to the data plotted in Fig. 4(b), within the experimental error bars, $(T_1T)^{-1}_{\rm anis} < 0$ at high temperatures, suggesting that $\varphi_3 > 0$.

As the magnetic transition is approached, the effects of the spin-orbit coupling presumably become more important. In particular, because in the magnetically ordered state the magnetic moments point parallel to the ordering vector $\mathbf{Q}_i$, ξ_1 must be the only correlation length that diverges at the magnetic transition, i.e., $\xi_1 \gg \xi_2, \xi_3$ at $T \gtrsim T_N$. Consequently, the first term in Eq. (4) should dominate in this regime. Because $\varphi_1 > 0$ and $A_{ab} < A_{aa}$, we expect that $(T_1T)^{-1}_{\rm anis} < 0$ near the transition. This expectation, however, does not agree with the observed behavior seen in Fig. 4(b).

We can also analyze the isotropic response, $\Delta(T_1T)^{-1}_{\rm iso}$. According to Eq. (5), $\Delta(T_1T)^{-1}_{\rm iso}$ is always positive. Indeed, neutron scattering experiments in both twinned [44] and detwinned [45] samples find enhanced magnetic fluctuations in the nematic phase. However, our data presented in Fig. 4(b) shows that $\Delta(T_1T)^{-1}_{\rm iso}$ is positive only at high temperatures—roughly within the same regime in which $(T_1T)^{-1}_{\rm anis} < 0$ – and becomes negative as T_N is approached, in contrast with the prediction of Eq. (5).

There are several possible reasons for this discrepancy between the theoretical calculation and the observed data in the temperature regime near T_N, including (i) unequal strain between the two different field orientations, (ii) crystal misalignments, and (iii) higher order corrections due to noninfinitesimal strain. Note that this device nominally applies a constant stress, rather than constant strain, and differential thermal contraction between the mechanical clamp, the silver wires, and the sample likely leads to a temperature-dependent induced strain. Because the nematic order parameters φ_i should be proportional to the strain, these quantities may not be the same for the two different field directions in the measured values. For example, if the wires used to suspend the sample exhibit a temperature-hysteretic effect due to thermal contractions that exceed the elastic regime, then the strain applied for the two different directions will be different.

Scenario (ii), crystal misalignment, could arise from a small component of $\mathbf{H}_0$ along the c direction that is different between different crystal orientations, which would contribute an asymmetry that would not cancel out. As the crystal is suspended in free space by the wires, it is possible that differences in thermal expansions could lead to torques that could twist the crystal, giving rise to a difference between the crystal orientation between strained and unstrained conditions. Detailed studies of the NMR spectra (not shown) in the ordered state of undoped $BaFe_2As_2$ under strain in this device indicate that misalignments of 1–2° are possible.

The third scenario, namely higher-order strain-induced changes to the spin-lattice relaxation rate, could be present, depending on the sensitivity of the nematic order parameters, φ_i, to strain. Nominally, the applied strains are small and are just enough to detwin the crystal. We observe little or no shift in the peak of $(T_1T)^{-1}_{\alpha}$ at T_N in Fig. 3, suggesting that the main effect of strain is to detwin the crystal. However, for sufficiently high strain levels, T_N is known to increase [45], and therefore the temperature dependence of the correlation lengths ξ_i will be altered.

In this regard, we note that the theoretical analysis presented here considers the linear response of $(T_1T)^{-1}_{\rm anis}$ to strain. From generic symmetry considerations, in the linear-response regime, one expects that $\Delta(T_1T)^{-1}_{a}$ and $\Delta(T_1T)^{-1}_{b}$ display opposite behaviors. From Fig. 4, this does seem to be the case at higher temperatures, where in fact the theoretical predictions for $(T_1T)^{-1}_{\rm anis}$ and $\Delta(T_1T)^{-1}_{\rm iso}$ are in qualitative agreement with the data. As T_N is approached, however, both $\Delta(T_1T)^{-1}_{a}$ and $\Delta(T_1T)^{-1}_{b}$ display the same behavior, indicating the onset of nonlinear effects beyond the analysis presented here. To mitigate these issues, it would be interesting to control precisely the applied strain using a piezo device, as it was done in Ref. [7] for resistivity measurements.

An alternative explanation for the inhomogeneity of the relaxation rates attributes it to the incommensurability of the magnetic ordering vector [46–48]. However, for the concentration studied here, high-resolution resonance magnetic x-ray diffraction reported no signs of incommensurability [49]. Neutron scattering studies have reported incommensurate order appears only at higher doping levels ($x > 0.056$) [50].

V. CONCLUSIONS

In summary, we have measured the NMR spin-lattice relaxation rate in $Ba(Fe_{1-x}Co_x)_2As_2$ with $x = 0.048$ under uniaxial tensile stress as a function of temperature and found significant changes to the relaxation rate that persist above T_s in a detwinned crystal. The strain field breaks C_4 symmetry, and the anisotropic magnetic fluctuations probed by T_1^{-1} reflect the impact of nematicity on the fluctuation spectrum. Surprisingly, the glassy behavior manifested by the broad distribution of relaxation times is unaffected under strain. This observation suggests that the local strains, introduced either by the Co dopants or by lattice defects, exceed the applied strain. Consequently the glassy behavior is not associated with large nematic domains.

We also compute the spin-lattice relaxation rate using a model for the anisotropic dynamical spin susceptibility. By introducing nematic order parameters that reflect the changes to the spin-spin correlation lengths along the three crystal axes, we estimate the leading contributions to the anisotropy of the spin-lattice relaxation rate in the presence of strain. Theoretically, we find that the strain-induced changes to $(T_1T)^{-1}_{a,b}$ should have opposite signs. On the other hand, experimentally we find that this is the case only at high temperatures, since both quantities are suppressed as T_N is approached. This discrepancy most likely arises due to crystal misalignments between the strained and unstrained states, and/or differences in induced strains between the two different directions. Future measurements with more precise control over the orientation and amplitude of the strain will provide detailed information about the relative sizes of the nematic order parameters, φ_i, under strain. Nevertheless, our experiments show that the combination of NMR and strain is a unique tool to probe the effect of nematic order not only on the unpolarized magnetic spectrum but most importantly on the polarized spin spectrum, revealing the interplay between nematicity and spin-orbit coupling.

ACKNOWLEDGMENTS

We thank S. Kivelson, E. Carlson, P. Pagliuso, and R. Urbano for enlightening discussions and P. Klavins, J. Crocker, K. Shirer, and M. Lawson for assistance in the laboratory. Work at UC Davis was supported by the NSF under Grant No. DMR-1506961. R.M.F. is supported by the US Department of Energy, Office of Science, Basic Energy Sciences, under Award No. DE-SC0012336. Work done at Ames Laboratory (S.L.B., P.C.C., M.T., R.P., E.I.T.) was supported by the US Department of Energy, Office of Basic Energy Science, Division of Materials Sciences and Engineering. Ames Laboratory is operated for the US Department of Energy by Iowa State University under Contract No. DE-AC02-07CH11358. This work was completed at the Aspen Center for Physics, which is supported by the National Science Foundation Grant No. PHY-1066293.

APPENDIX: DETAILS OF THE CALCULATION OF THE ANISOTROPIC SPIN-LATTICE RELAXATION RATE

Equation (1) of the main text contains the hyperfine tensor

$$\bar{A}_{\mathbf{q}} = 4\begin{pmatrix} A_{aa}\cos\left(\frac{q_x}{2}\right)\cos\left(\frac{q_y}{2}\right) & -A_{ab}\sin\left(\frac{q_x}{2}\right)\sin\left(\frac{q_y}{2}\right) & iA_{ac}\sin\left(\frac{q_x}{2}\right)\cos\left(\frac{q_y}{2}\right) \\ -A_{ba}\sin\left(\frac{q_x}{2}\right)\sin\left(\frac{q_y}{2}\right) & A_{bb}\cos\left(\frac{q_x}{2}\right)\cos\left(\frac{q_y}{2}\right) & iA_{bc}\cos\left(\frac{q_x}{2}\right)\sin\left(\frac{q_y}{2}\right) \\ iA_{ca}\sin\left(\frac{q_x}{2}\right)\cos\left(\frac{q_y}{2}\right) & iA_{cb}\cos\left(\frac{q_x}{2}\right)\sin\left(\frac{q_y}{2}\right) & A_{cc}\cos\left(\frac{q_x}{2}\right)\cos\left(\frac{q_y}{2}\right) \end{pmatrix}$$

and the rotation matrix

$$\bar{R} = \begin{pmatrix} \sin^2\phi + \cos\theta\,\cos^2\phi & -\sin 2\phi\,\sin^2\frac{\theta}{2} & \cos\phi\,\sin\theta \\ -\sin 2\phi\,\sin^2\frac{\theta}{2} & \cos^2\phi + \cos\theta\,\sin^2\phi & \sin\phi\,\sin\theta \\ -\cos\phi\,\sin\theta & -\sin\phi\,\sin\theta & \cos\theta \end{pmatrix}.$$

Using Eq. (1), we can also calculate $1/T_1T$ for a field applied parallel to c:

$$\left(\frac{1}{T_1T}\right)_c = \frac{g^2}{2}\sum_{\mathbf{q}}\left\{\left[\sin^2\left(\frac{q_x}{2}\right)\sin^2\left(\frac{q_y}{2}\right)A_{ab}^2 + \cos^2\left(\frac{q_x}{2}\right)\cos^2\left(\frac{q_y}{2}\right)A_{aa}^2\right][\tilde{\chi}_{aa}(\mathbf{q}) + \tilde{\chi}_{bb}(\mathbf{q})] + \frac{1}{2}[1-\cos(q_x)\cos(q_y)]A_{ac}^2\tilde{\chi}_{cc}(\mathbf{q})\right\} \tag{A1}$$

as well as the isotropic response $(T_1T)_{\rm iso}^{-1} = (T_1T)_a^{-1} + (T_1T)_b^{-1}$:

$$\left(\frac{1}{T_1T}\right)_a + \left(\frac{1}{T_1T}\right)_b = \frac{g^2}{2}\sum_{\mathbf{q}}\left\{\left[\sin^2\left(\frac{q_x}{2}\right)\sin^2\left(\frac{q_y}{2}\right)A_{ab}^2 + \cos^2\left(\frac{q_x}{2}\right)\cos^2\left(\frac{q_y}{2}\right)A_{aa}^2 + \frac{1}{2}\left(1-\cos q_x\cos q_y\right)A_{ca}^2\right][\tilde{\chi}_{aa}(\mathbf{q}) + \tilde{\chi}_{bb}(\mathbf{q})] - \left[\frac{1}{2}\left(\cos q_x - \cos q_y\right)A_{ca}^2\right](\tilde{\chi}_{aa}(\mathbf{q}) - \tilde{\chi}_{bb}(\mathbf{q})) + \left[\frac{1}{2}\left(1-\cos q_x\cos q_y\right)A_{ac}^2 + 2\cos^2\left(\frac{q_x}{2}\right)\cos^2\left(\frac{q_y}{2}\right)A_{cc}^2\right]\tilde{\chi}_{cc}(\mathbf{q})\right\}. \tag{A2}$$

Focusing on the behavior at the magnetic ordering vectors $\mathbf{Q}_1 = (\pi,0)$ and $\mathbf{Q}_2 = (0,\pi)$, we note that $(T_1T)_c^{-1}$ is dominated by the out-of-plane fluctuations, $\chi_{cc}(\mathbf{Q}_i)$, whereas $(T_1T)_{\rm iso}^{-1}$ contains also contributions from $\chi_{aa}(\mathbf{Q}_1)$ and $\chi_{bb}(\mathbf{Q}_2)$.

[1] P. C. Canfield and S. L. Bud'ko, FeAs-based superconductivity: A case study of the effects of transition metal doping on $BaFe_2As_2$, Annu. Rev. Condens. Matter Phys. **1**, 27 (2010).

[2] D. C. Johnston, The puzzle of high temperature superconductivity in layered iron pnictides and chalcogenides, Adv. Phys. **59**, 803 (2010).

[3] T. Moriya and K. Ueda, Antiferromagnetic spin fluctuations and superconductivity, Rep. Prog. Phys. **66**, 1299 (2003).

[4] A. Chubukov, Pairing mechanism in Fe-based superconductors, Annu. Rev. Condens. Matter Phys. **3**, 57 (2012).

[5] S. Lederer, Y. Schattner, E. Berg, and S. A. Kivelson, Enhancement of Superconductivity Near a Nematic Quantum Critical Point, Phys. Rev. Lett. **114**, 097001 (2015).

[6] T. A. Maier and D. J. Scalapino, Pairing interaction near a nematic quantum critical point of a three-band cuo_2 model, Phys. Rev. B **90**, 174510 (2014).

[7] J.-H. Chu, H.-H. Kuo, J. G. Analytis, and I. R. Fisher, Divergent nematic susceptibility in an iron arsenide superconductor, Science **337**, 710 (2012).

[8] R. M. Fernandes, A. V. Chubukov, J. Knolle, I. Eremin, and J. Schmalian, Preemptive nematic order, pseudogap, and orbital order in the iron pnictides, Phys. Rev. B **85**, 024534 (2012).

[9] E. Fradkin, S. A. Kivelson, M. J. Lawler, J. P. Eisenstein, and A. P. Mackenzie, Nematic fermi fluids in condensed matter physics, Annu. Rev. Condens. Matter Phys. **1**, 153 (2010).

[10] R. M. Fernandes, A. V. Chubukov, and J. Schmalian, What drives nematic order in iron-based superconductors?, Nat. Phys. **10**, 97 (2014).

[11] C. de la Cruz, Q. Huang, J. W. Lynn, Jiying Li, W. Ratcliff II, J. L. Zarestky, H. A. Mook, G. F. Chen, J. L. Luo, N. L. Wang, and P. Dai, Magnetic order close to superconductivity in the iron-based layered $LaO_{1-x}F_xFeAs$ systems, Nature (London) **453**, 899 (2008).

[12] P. Dai, Antiferromagnetic order and spin dynamics in iron-based superconductors, Rev. Mod. Phys. **87**, 855 (2015).

[13] M. A. Tanatar, A. Kreyssig, S. Nandi, N. Ni, S. L. Bud'ko, P. C. Canfield, A. I. Goldman, and R. Prozorov, Direct imaging of the structural domains in the iron pnictides $AFe_2As_2(A = Ca, Sr, Ba)$, Phys. Rev. B **79**, 180508 (2009).

[14] E. C. Blomberg, A. Kreyssig, M. A. Tanatar, R. M. Fernandes, M. G. Kim, A. Thaler, J. Schmalian, S. L. Bud'ko, P. C. Canfield, A. I. Goldman, and R. Prozorov, Effect of tensile stress on the in-plane resistivity anisotropy in $BaFe_2As_2$, Phys. Rev. B **85**, 144509 (2012).

[15] J.-H. Chu, J. G. Analytis, K. De Greve, P. L. McMahon, Z. Islam, Y. Yamamoto, and I. R. Fisher, In-plane resistivity anisotropy in an underdoped iron arsenide superconductor, Science **329**, 824 (2010).

[16] M. A. Tanatar, E. C. Blomberg, A. Kreyssig, M. G. Kim, N. Ni, A. Thaler, S. L. Bud'ko, P. C. Canfield, A. I. Goldman, I. I. Mazin, and R. Prozorov, Uniaxial-strain mechanical detwinning of $CaFe_2As_2$ and $BaFe_2As_2$ crystals: Optical and transport study, Phys. Rev. B **81**, 184508 (2010).

[17] X. Lu, J. T. Park, R. Zhang, H. Luo, A. H. Nevidomskyy, Q. Si, and P. Dai, Nematic spin correlations in the tetragonal state of uniaxial-strained $BaFe_{2-x}Ni_xAs_2$, Science **345**, 657 (2014).

[18] H. Man, X. Lu, J. S. Chen, R. Zhang, W. Zhang, H. Luo, J. Kulda, A. Ivanov, T. Keller, E. Morosan, Q. Si, and P. Dai, Electronic nematic correlations in the stress-free tetragonal state of $BaFe_{2-x}Ni_xAs_2$, Phys. Rev. B **92**, 134521 (2015).

[19] X. Lu, K.-F. Tseng, T. Keller, W. Zhang, D. Hu, Y. Song, H. Man, J. T. Park, H. Luo, S. Li *et al.*, Impact of uniaxial pressure on structural and magnetic phase transitions in electron-doped iron pnictides, Phys. Rev. B **93**, 134519 (2016).

[20] M. Yi, D. Lu, J.-H. Chu, J. G. Analytis, A. P. Sorini, A. F. Kemper, B. Moritz, S.-K. Mo, R. G. Moore, M. Hashimoto *et al.*, Symmetry-breaking orbital anisotropy observed for detwinned $Ba(Fe_{1-x}Co_x)_2As_2$ above the spin density wave transition, Proc. Natl. Acad. Sci. U.S.A. **108**, 6878 (2011).

[21] C. Mirri, A. Dusza, S. Bastelberger, M. Chinotti, L. Degiorgi, J.-H. Chu, H.-H. Kuo, and I. R. Fisher, Origin of the Resistive Anisotropy in the Electronic Nematic Phase of $BaFe_2As_2$ Revealed by Optical Spectroscopy, Phys. Rev. Lett. **115**, 107001 (2015).

[22] K. Kitagawa, N. Katayama, K. Ohgushi, and M. Takigawa, Antiferromagnetism of $SrFe_2As_2$ studied by single-crystal ^{75}As-NMR, J. Phys. Soc. Jpn. **78**, 063706 (2009).

[23] K. Kitagawa, N. Katayama, K. Ohgushi, M. Yoshida, and M. Takigawa, Commensurate itinerant antiferromagnetism in $BaFe_2As_2$: ^{75}As-NMR studies on a self-flux grown single crystal, J. Phys. Soc. Jpn. **77**, 114709 (2008).

[24] F. L. Ning, K. Ahilan, T. Imai, A. S. Sefat, M. A. McGuire, B. C. Sales, D. Mandrus, P. Cheng, B. Shen, and H.-H Wen, Contrasting Spin Dynamics between Underdoped and Overdoped $Ba(Fe_{1-x}Co_x)_2As_2$, Phys. Rev. Lett. **104**, 037001 (2010).

[25] F. L. Ning, K. Ahilan, T. Imai, A. S. Sefat, R. Jin, M. A. McGuire, B. C. Sales, and D. Mandrus, ^{59}Co and ^{75}As NMR investigation of lightly doped $Ba(Fe_{1-x}Co_x)_2As_2$ ($x = 0.02, 0.04$), Phys. Rev. B **79**, 140506 (2009).

[26] T. Iye, M.-H. Julien, H. Mayaffre, M. Horvatić, C. Berthier, K. Ishida, H. Ikeda, S. Kasahara, T. Shibauchi, and Y. Matsuda, Emergence of orbital nematicity in the tetragonal phase of $BaFe_2(As1 - xP_x)_2$, J. Phys. Soc. Jpn. **84**, 043705 (2015).

[27] Y. Nakai, T. Iye, S. Kitagawa, K. Ishida, S. Kasahara, T. Shibauchi, Y. Matsuda, H. Ikeda, and T. Terashima, Normal-state spin dynamics in the iron-pnictide superconductors $BaFe_2(As_{1-x}P_x)_2$ and $Ba(Fe_{1-x}Co_x)_2As_2$ probed with NMR measurements, Phys. Rev. B **87**, 174507 (2013).

[28] Y. Nakai, T. Iye, S. Kitagawa, K. Ishida, H. Ikeda, S. Kasahara, H. Shishido, T. Shibauchi, Y. Matsuda, and T. Terashima, Unconventional Superconductivity and Antiferromagnetic Quantum Critical Behavior in the Isovalent-Doped $BaFe_2(As_{1-x}P_x)_2$, Phys. Rev. Lett. **105**, 107003 (2010).

[29] F. L. Ning, M. Fu, D. A. Torchetti, T. Imai, A. S. Sefat, P. Cheng, B. Shen, and H.-H. Wen, Critical behavior of the spin density wave transition in underdoped $Ba(Fe_{1-x}Co_x)_2As_2$ ($x \leqslant 0.05$): ^{75}As NMR investigation, Phys. Rev. B **89**, 214511 (2014).

[30] A. P. Dioguardi, M. M. Lawson, B. T. Bush, J. Crocker, K. R. Shirer, D. M. Nisson, T. Kissikov, S. Ran, S. L. Bud'ko, P. C. Canfield, S. Yuan, P. L. Kuhns, A. P. Reyes, H.-J. Grafe, and N. J. Curro, NMR evidence for inhomogeneous glassy behavior driven by nematic fluctuations in iron arsenide superconductors, Phys. Rev. B **92**, 165116 (2015).

[31] H.-J. Grafe, U. Gräfe, A. P. Dioguardi, N. J. Curro, S. Aswartham, S. Wurmehl, and B. Buchner, Identical spin fluctuations in Cu- and Co-doped $BaFe_2As_2$ independent of electron doping, Phys. Rev. B **90**, 094519 (2014).

[32] A. P. Dioguardi, J. Crocker, A. C. Shockley, C. H. Lin, K. R. Shirer, D. M. Nisson, M. M. Lawson, N. apRoberts-Warren, P. C. Canfield, S. L. Bud'ko, S. Ran, and N. J. Curro, Coexistence of Cluster Spin Glass and Superconductivity in $Ba(Fe_{1-x}Co_x)_2As_2$ for $0.060 \leqslant x \leqslant 0.071$, Phys. Rev. Lett. **111**, 207201 (2013).

[33] A. P. Dioguardi, N. apRoberts-Warren, A. C. Shockley, S. L. Bud'ko, N. Ni, P. C. Canfield, and N. J. Curro, Local magnetic inhomogeneities in $Ba(Fe_{1-x}Ni_x)_2As_2$ as seen via ^{75}As NMR, Phys. Rev. B **82**, 140411(R) (2010).

[34] N. Ni, M. E. Tillman, J.-Q. Yan, A. Kracher, S. T. Hannahs, S. L. Bud'ko, and P. C. Canfield, Effects of Co substitution on thermodynamic and transport properties and anisotropic H_{c2} in $Ba(Fe_{1-x}Co_x)_2As_2$ single crystals, Phys. Rev. B **78**, 214515 (2008).

[35] D. C. Johnston, Stretched exponential relaxation arising from a continuous sum of exponential decays, Phys. Rev. B **74**, 184430 (2006).

[36] K. Park, D. Louca, A. Llobet, and J.-Q. Yan, Evidence of local disorder in the overdoped regime of $Ba(Fe_{1-x}Co_x)_2As_2$, Phys. Rev. B **84**, 024512 (2011).

[37] A. Smerald and N. Shannon, Angle-resolved NMR: Quantitative theory of ^{75}As T_1 relaxation rate in $BaFe_2As_2$, Phys. Rev. B **84**, 184437 (2011).

[38] S. V. Borisenko, D. V. Evtushinsky, Z.-H. Liu, I. Morozov, R. Kappenberger, S. Wurmehl, B. Bchner, A. N. Yaresko, T.

K. Kim, M. Hoesch *et al.*, Direct observation of spin-orbit coupling in iron-based superconductors, Nat. Phys. **12**, 311 (2015).

[39] V. Cvetkovic and O. Vafek, Space group symmetry, spin-orbit coupling, and the low-energy effective Hamiltonian for iron-based superconductors, Phys. Rev. B **88**, 134510 (2013).

[40] M. H. Christensen, J. Kang, B. M. Andersen, I. Eremin, and R. M. Fernandes, Spin reorientation driven by the interplay between spin-orbit coupling and Hund's rule coupling in iron pnictides, Phys. Rev. B **92**, 214509 (2015).

[41] D. S. Inosov, J. T. Park, P. Bourges, D. L. Sun, Y. Sidis, A. Schneidewind, K. Hradil, D. Haug, C. T. Lin, B. Keimer *et al.*, Normal-state spin dynamics and temperature-dependent spin-resonance energy in optimally doped $BaFe_{1.85}$ $Co_{0.15}$ As_2, Nat. Phys. **6**, 178 (2009).

[42] G. S. Tucker, R. M. Fernandes, H.-F. Li, V. Thampy, N. Ni, D. L. Abernathy, S. L. Bud'ko, P. C. Canfield, D. Vaknin, J. Schmalian *et al.*, Magnetic excitations in underdoped $Ba(Fe_{1-x}Co_x)_2As_2$ with $x = 0.047$, Phys. Rev. B **86**, 024505 (2012).

[43] R. M. Fernandes and J. Schmalian, Manifestations of nematic degrees of freedom in the magnetic, elastic, and superconducting properties of the iron pnictides, Supercond. Sci. Technol. **25**, 084005 (2012).

[44] Q. Zhang, R. M. Fernandes, J. Lamsal, J. Yan, S. Chi, G. S. Tucker, D. K. Pratt, J. W. Lynn, R. W. McCallum, P. C. Canfield, T. A. Lograsso, A. I. Goldman, D. Vaknin, and R. J. McQueeney, Neutron-Scattering Measurements of Spin Excitations in LaFeAsO and $Ba(Fe_{0.953}Co_{0.047})_2As_2$: Evidence for a Sharp Enhancement of Spin Fluctuations by Nematic Order, Phys. Rev. Lett. **114**, 057001 (2015).

[45] C. Dhital, T. Hogan, Z. Yamani, R. J. Birgeneau, W. Tian, M. Matsuda, A. S. Sefat, Z. Wang, and S. D. Wilson, Evolution of antiferromagnetic susceptibility under uniaxial pressure in $Ba(Fe_{1-x}Co_x)_2As_2$, Phys. Rev. B **89**, 214404 (2014).

[46] Y. Laplace, J. Bobroff, F. Rullier-Albenque, D. Colson, and A. Forget, Atomic coexistence of superconductivity and incommensurate magnetic order in the pnictide $Ba(Fe_{1-x}Co_x)_2As_2$, Phys. Rev. B **80**, 140501 (2009).

[47] P. Bonville, F. Rullier-Albenque, D. Colson, and A. Forget, Incommensurate spin density wave in Co-doped $BaFe_2As_2$, EPL **89**, 67008 (2010).

[48] L. P. Gor'kov and G. B. Teitel'baum, Spatial inhomogeneities in iron pnictide superconductors: The formation of charge stripes, Phys. Rev. B **82**, 020510 (2010).

[49] M. G. Kim, A. Kreyssig, Y. B. Lee, J. W. Kim, D. K. Pratt, A. Thaler, S. L. Bud'ko, P. C. Canfield, B. N. Harmon, R. J. McQueeney, and A. I. Goldman, Commensurate antiferromagnetic ordering in $Ba(Fe_{1-x}Co_x)_2As_2$ determined by x-ray resonant magnetic scattering at the Fe *K* edge, Phys. Rev. B **82**, 180412(R) (2010).

[50] D. K. Pratt, M. G. Kim, A. Kreyssig, Y. B. Lee, G. S. Tucker, A. Thaler, W. Tian, J. L. Zarestky, S. L. Bud'ko, P. C. Canfield, B. N. Harmon, A. I. Goldman, and R. J. McQueeney, Incommensurate Spin-Density Wave Order in Electron-Doped $BaFe_2As_2$ Superconductors, Phys. Rev. Lett. **106**, 257001 (2011).